International Journal of Pharmaceutics 663 (2024) 124553

Contents lists available at ScienceDirect

International Journal of Pharmaceutics

journal homepage: www.elsevier.com/locate/ijpharm

A Natural deep eutectic solvent as an effective material for dual debridement and antibiofilm effects in chronic wound treatment

Christina MAP Schuh [a,1], Fernando Ezquer [a,1], Sigde Mamani [b], Paola R. Campodónico [b], Constanza Cárcamo [b], Fabián Martinez-Gómez [c], Isabel Aburto [d], Marcelo Ezquer [a], Bernardo Morales [e], Belén Olivares [b,*]

[a] Centro de Medicina Regenerativa, Facultad de Medicina, Clínica Alemana-Universidad del Desarrollo, Santiago, Chile
[b] Centro de Química Medica, Facultad de Medicina, Clínica Alemana-Universidad del Desarrollo, Santiago, Chile
[c] Laboratorio de Resonancia Magnética Nuclear, Universidad de Santiago de Chile, Santiago, Chile
[d] Fundación Instituto Nacional de Heridas, Santiago, Chile
[e] Facultad de Salud, Universidad del Alba, Santiago, Chile

ARTICLE INFO

Keywords:
Chronic wounds
Biofilm
Debridement
Deep eutectic solvent
Wound dressing

ABSTRACT

In chronic wound treatment, the debridement of devitalized tissue and the eradication of the biofilm must balance aggressiveness with care to protect regenerating tissues. In this study, urea, a potent chaotropic molecule, was modulated through the formation of a Natural Deep Eutectic Solvent (NADES) with betaine to develop a new debriding material (BU) suitable for application into injured dermal tissues. To evaluate BU's debriding capacity, along with its antibiofilm effect and biocompatibility, pre-clinical to clinical methods were employed. In vitro determinations using artificial and clinical slough samples indicate that BU has a high debriding capacity. Additionally, BU's de-structuring effects lead to a strong antibiofilm capability, demonstrated by a reduced bacterial load compared to the antiseptic PHMB-Betaine or medical honey, evaluated in artificial slough and *ex vivo* human skin. Furthermore, BU's efficacy was evaluated in a murine model of diabetic wound, demonstrating significant effects on debriding and antibiofilm capacity, similar to those observed in PHMB-Betaine and medical honey-treated animals. Finally, BU was clinically evaluated in leg ulcers, showing superiority in reduction of bacterial load and wound area compared to honey, with no adverse effects. Thus, BU represents a simple and non-biocidal option that could contributes to chronic wound care.

1. Introduction

Chronic wounds represent a challenging therapeutic condition where tissue regeneration is halted due to multiple pathological factors (Milne et al., 2020). These factors hinder the normal progression towards healing, often leaving the process stalled in an inflammatory state characterized by the high production of devitalized tissue known as slough (Eriksson et al., 2022; Milne, 2015; Section 2, 2022). Slough is a cross-linked proteinaceous matrix primarily composed of collagen, fibrin, and elastin, together with cellular debris and serum exudates, commonly present in chronic wounds. This environment is optimal for rapid bacterial colonization, intensifying the inflammatory state and creating a vicious cycle that prevents the healing process (Percival and Suleman, 2015).

On the other hand, bacteria in chronic wounds mainly exist in a biofilm form, which exhibits tolerance to the host's immune system, antibiotics, and many antibacterial antiseptic products. This increased tolerance is because in biofilms, bacteria are embedded in a protected environment provided by the extracellular bacterial matrix, preventing them from being effectively targeted (Bjarnsholt et al., 2008; Sen et al., 2021).

It is clinically recognized that removing the colonized slough and others devitalized tissue is mandatory to favour wound closure (Eriksson et al., 2022; The rationale for wound hygiene, 2020). Debridement represents the clinical strategy to remove devitalized tissue from open chronic wounds and has been considered the most effective intervention for cleaning the wound bed. Debridement removes both: the biofilm together with its support, the devitalized tissue, simultaneously

* Corresponding autor at: Facultad de Medicina.Clínica Alemana, Universidad del Desarrollo, Avenida Plaza 680, Las Condes, Santiago de, Chile.
E-mail address: molivares@udd.cl (B. Olivares).
[1] Contributed equally to this work.

https://doi.org/10.1016/j.ijpharm.2024.124553
Received 23 June 2024; Received in revised form 28 July 2024; Accepted 2 August 2024
Available online 3 August 2024

(Thomas et al., 2021). There are different debridement approaches: enzymatically, using proteolytic enzymes; osmotically, by applying hyperosmotic products that induce the patient's own proteolytic enzymes to flow out of vessels and act on the wound bed; and finally, mechanically using medical tools. However, they harbour some disadvantages. For example, mechanical methods cause high levels of pain and require anaesthesia, while enzymatic and osmotic products are slow and are associated with irritation and maceration of the wound edges (Swanson et al., 2022). The evidence points to the strong benefits of debridement; however, there is considerable scope to develop new effective materials to improve the available clinical strategies (Lewis et al., 2001; Woo et al., 2015).

Natural Deep Eutectic Solvents (NADESs) are formed by mixing solid substances that, in certain proportions, can interact intermolecularly to form a supramolecular network. This is achieved through hydrogen bond interactions, generating a liquid deep eutectic mixture with a melting point much lower than the original components (Martins et al., 2019). NADESs offer an opportunity to combine the individual and distinct physicochemical properties of their constituents with the unique supramolecular ordering achieved through the eutectic microstructure. The physicochemical properties of NADESs can be adjusted to the required aims through changes in the composition and/or proportion of its components, representing designer liquids. Furthermore, the synthesis techniques are very simple, non-polluting, economical, and easily scalable (Aroso et al., 2017; Liu et al., 2018). Combined with the favourable biocompatibility profile achieved in NADESs composed of physiological metabolites, there is a valuable potential to explore new applications in the biomaterial and biomedical fields.

In the present work, taking advantage of the of design flexibility of NADESs, a new debriding formulation was prepared and studied for application in chronic wound treatment (Sun et al., 2023; Liu et al., 2022). Urea, a potent chaotropic molecule often used as keratolytic in epidermal tissues was selected and its potency was modulated through NADES formation with betaine to obtain the debriding agent (BU), that could be applicable to dermic sensible tissues (Celleno, 2018). On the other hand, betaine was selected based on its known capacity to form NADESs with several hydrogen bond donors (Abranches et al., 2020). The physicochemical characteristics of BU, together with its debriding and antibiofilm properties were extensively studied using in vitro, *ex vivo, in vivo* animal models and through a pilot clinical evaluation.

2. Materials and methods

2.1. NADES preparation and characterization

2.1.1. NADES preparation

The liquid formula was obtained by the agitation-heating method, at 200 rpm and 70 °C in a round- bottom flask, mixing betaine (betaine monohydrate, Santa Cruz Biotech) as the hydrogen bonding acceptor and urea (Urea OmniPur® Merck) as the hydrogen bond donor. The molar ratio of Betaine:Urea was 1:1.5. Water was included in 14 % w/w to confer stability. The formula was identified as BU and was sterilized by filtration using 0.22 μm membrane filters and kept in a tightly closed tube until use.

2.1.2. Thermal characterization of BU

Differential scanning calorimetry was performed with a Perkin Elmer DSC4000 equipment. Samples were weighed (6–12 mg) and placed in the equipment's sealed sample pan. All measurements were performed under an ultra-pure gaseous nitrogen flow of 20 mL/min. The cooling and heating rate was set at 1 °C/min, and measurements were conducted in the temperature range of −79 °C to 121 °C (Zheng et al., 2019).

The thermogravimetric analysis (TGA) experiments were carried out using a Perkin Elmer STA, model 8000. For the experiment, 11.5 mg of the sample was weighed, transferred to a sample pan and placed in the equipment. The experiments were conducted with an extra pure nitrogen flow of 20 mL/min, with a heating rate of 15 °C/min until reaching 300 °C (Chen et al., 2018).

2.1.3. Hygroscopicity and water content measurements

Hygroscopicity was evaluated by maintaining BU aliquots in three humidity conditions: 11 %, 25 % and 50 % relative humidity (% RH) using a temperature and humidity-controlled chamber (MMM® Climacell 222-Eco). After experiments, samples were kept in tightly closed tubes until analysis of water content performed through Karl Fisher titration method (Hanna® Karl Fisher HI933) (Shishov et al., 2023).

2.2. In vitro assessment of BU debriding potential: Slough disorganization model

2.2.1. Evaluation of in vitro slough de-structuring capacity

An artificial wound slough model was adapted from a previous report (Shi et al., 2009). For that purpose, a matrix gel of collagen (rat tail collagen type I in acetic acid, 3.1 mg/mL, Gibco), fibrinogen from human plasma (25 mg/mL, Sigma), and elastin (10 mg/mL; Sigma) was prepared as follows: In pre-chilled tubes, 650 μL of collagen was mixed with 10X phosphate-buffered saline (PBS) and 150 μL of fibrinogen. Subsequently, 0.14 mg/mL of previously labelled elastin (Alexa Fluor 488 protein Labeling Kit – A10235 Invitrogen) was added and gently mixed. Then, 25 μL of 1 N NaOH was added to neutralize the solution. Finally, 25 μL of thrombin (10 UI/mL dissolved in 40 mM $CaCl_2$) was added. 200 μL of the mixture were placed in a 96-wells plate and incubated for 1 h at 37 °C. The gels were maintained at 4 °C for 24 h prior to use. In the subsequent paragraphs, gels are referred to as "artificial slough".

Artificial slough disorganization was assessed with two different methods: ultraviolet spectroscopy to quantify changes in the matrix organization (Ran et al., 2021), and fluorescence measurement of eluted proteins (based on Alexa Fluor 488-labelled elastin) (Shi et al., 2009). For ultraviolet spectroscopy, artificial slough was treated with 50 μL of BU and placed into a microplate reader (Cytation™3, BioTek®, US) for 3 h at RT. Saline solution (NaCl 0.9 %, Biosano) and collagenase solution (500 μg/mL) were used as controls. For the protein elution measurement, transwell inserts (NEST Insert 725,301 24-well plates 8.0 μm polycarbonate membrane) were used. The artificial slough matrix was placed into the transwell insert and treated as described above. The receptor chamber contained 200 μL of PBS. The fluorescence of the receptor chamber solution (Excitation 485 nm, Emission 528 nm) was measured before treatments and at 0.25, 0.5, 0.75, 1.0, 1.15, 1.5, 2.0, 3.0, 4.0 and 24 h after treatment in a microplate reader (Cytation™3 BioTek®).

2.2.2. Evaluation of in vitro slough swelling capacity

The artificial sloughs and clinical sloughs obtained from disposal clinical samples (Approved by the Scientific Ethics Committee at Fundación Instituto Nacional de Heridas Protocol 427605_05112021) were lyophilized, weighted, and then allowed to hydrate 24 h in excess of PBS or BU at 35 °C using a thermoplate (Thermomix® mLab Scientific). The weights of the hydrated samples were measured at 0, 5, 10, 15, 20, 25, 30, 60, 100, 130, 220 and 1440 min, following removal of excess liquids by gentle blotting with a paper towel. The percentage of solvent uptake was measured as a surrogate of slough swelling (% solvent uptake) and calculated as previously reported (Flayhart et al., 2004) by the following equation:

$$\%\,\text{Solvent uptake} = \frac{Ws - Wd}{Wd} x100$$

where Ws and Wd are the weights of the swollen and dried slough, respectively.

2.3. In vitro mixed biofilm model

The artificial slough was used to emulate the proteinaceous support to culture bacterial biofilm on it. Artificial sloughs in transwell inserts were placed into plate-wells as receptor chambers containing 200 μL of Dulbeccós Modified Eagle medium (DMEM, high glucose, pyruvate Gibco®). Media was renewed every 24 h.

For generation of the mixed biofilm model, *Staphilococcus aureus (S. aureus* ATCC-29213*)* and *Pseudomonas aeruginosa* (*P. aeruginosa* ATCC-27853) were grown in Luria Bertani Broth under 100 rpm agitation for 3 h. Prior to experimentation, aliquots of the broth were resuspended in PBS, and the McFarland value was adjusted with the spectrophotometer (Agilent® 8453), resulting in 1×10^8 CFU/mL. Then, individual bacterial solutions were mixed at a 1:1 ratio to a final concentration of $1x10^6$ CFU/mL, and 25 μL of this suspension was cultured in triplicate on the artificial slough. Biofilms were left to mature at 37 °C for 24, 48 or 72 h, and subsequently treated with 50 μL of saline (NaCl 0,9%), BU, Manuka Honey (Therahoney®), subsequently named Honey or a polyhexanide-betaine antiseptic solution (Prontosan® B Braun) subsequently named PHMB-Betaine, for 24 h. Subsequently, gels were rinsed twice to remove planktonic bacteria, and the solid matrix was placed in a tube containing 300 μl PBS. Tubes were subjected to horizontal agitation at 15 °C in cycles of 950 rpm and then at 1400 rpm for 20 min each. 100 μL of the resulting bacterial suspension was diluted in 1:10 dilution series in 1 mL of PBS. Then, 100 μL of the dilutions were plated on CHROMagar Orientation® (Becton Dickinson) and incubated overnight at 37 °C. For counting, *P. aeruginosa* was identified as transparent, yellow serrated and diffuse edges, and selectively differentiated from *S. aureus,* presenting opaque white to smaller yellowish colonies (Flayhart et al., 2004).

2.4. Human ex vivo mixed biofilm model

Human skin explants were obtained from cosmetic surgeries. The local ethics review board (Scientific Ethics Committee for Health Sciences at Pontificia Universidad Católica de Chile, No. 210326005) approved the collection of skin tissue, after obtaining written informed consent for each donor. The *ex vivo* model comprised circular skin sections prepared after hypodermal fat elimination. A partial-thickness wound was induced using a 5 mm diameter biopsy punch. The explants were transferred into a transwell insert with the dermis facing downward and placed in the plate well in contact with 200 μL DMEM (DMEM, high glucose, pyruvate Gibco®) as previously reported (Garcia-Bilbao et al., 2020). The bacterial suspension was prepared as described above, and 25 μL of PBS containing $1x10^8$ CFU/mL of *P. aeruginosa* and *S. aureus*, in a 1:1 proportion, were loaded onto the explants. Biofilms were grown for 24, 48 or 72 h, and subsequently treated with 50 μL of saline, BU, Honey, or PHMB-Betaine for 24 h. Subsequently, the explants were rinsed with PBS to remove planktonic cells and processed for viable bacterial quantification as described above.

2.5. Murine diabetic biofilm model in full-thickness wounds

The *in vivo* anti-biofilm activity of BU was evaluated in a model of streptozotocin-induced diabetes in C57BL/6 mice. This model has been shown to resemble the wound healing and biofilm colonization complication observed in humans (Krishnan et al., 2018; Ezquer et al., 2015). Experiments were approved by the local Animal Committee in accordance with the Chilean law (CICUAL No: N°7/2022), ARRIVE guidelines, and 3R practices. C57BL/6 mice were kept in an enriched environment with a 12 h/12 h light/dark cycle, at 23–25 °C temperature, with access to food and water ad libitum. For experimentation, 10-week-old male and female mice were utilized. The well-being of animals throughout experimentation was assessed daily using the standardized "Morton and Griffith" assessment and the Grimace scale.

2.5.1. Induction of diabetes with streptozotocin

For diabetes induction, mice were deeply anesthetized with sevoflurane (at 3 % in a flow rate of 3–5 L per minute of medical oxygen), and 200 mg/kg streptozotocin dissolved in 0.1 M citrate buffer at pH 4.5 was injected intraperitoneally after 8 h of fasting. After streptozotocin administration, diabetes induction was evaluated every three days by taking blood from the tail vein of animals and measuring blood glucose levels with a portable glucometer (OneTouch Select Plus Flex® MEDCORP SA). Animals were considered diabetic when glycemic levels were ≥300 mg/dL in two consecutives measurements (Ezquer et al., 2015).

2.5.2. Full thickness wound model with bacterial biofilm

Before generating the full-thickness wounds, animals were randomly assigned to their respective groups (Saline, BU, Honey, or PHMB-Betaine). Thirteen days after diabetes induction mice were deeply anesthetized by inhalation of sevoflurane, and their upper dorsum was depilated. Then, a 6 mm full-thickness wound was generated in the neck area using a sterile biopsy punch. To prevent wound contraction, a silicone splint (Grace Bio-Labs 476687) was placed around the wound with skin adhesive and six sutures (vicryl 5–0). Wounds were covered with Tegaderm film to avoid infection, and analgesics were given once a day for 3 days post-surgery (meloxicam, 2 mg/kg).

Twenty-four hours after wound infliction, bacteria were inoculated into the wounds by applying 25 μL of a $1x10^8$ CFU/ml solution of *P. aeruginosa* and *S. aureus* and the wounds were covered with Tegaderm. After 48 h, a bacterial biofilm was established, which was verified in the group identified as "initial" (n = 3) both by its macroscopic characteristics and bacterial load analysis. The wound and the formed biofilm were treated every 48 h for 7 days by applying the following steps: i) brief anesthesia with sevoflurane for immobilization, ii) cleaning the exudate and planktonic bacteria by rinsing with 25 μL of saline, iii) application of 25 μL of the corresponding treatment product, and iv) covering the wound with Tegaderm® dressing. After 24 h of the last treatment, animals were euthanized by intraperitoneal administration of ketamine 500 mg/Kg and Xylazine 100 mg/Kg intraperitoneal. Eight millimeters skin samples were taken encompassing the entire wound area concentrically, using a biopsy punch after the holding ring was removed. Each sample was divided into two equal parts, one for bacterial counting, utilizing the method described above, and the other for fixation in 4 % paraformaldehyde and paraffin embedding for histological analysis.

2.6. Assessment of BU biocompatibility

2.6.1. BU cytotoxicity and immunogenicity assays

BU cytotoxicity was evaluated in vitro using the keratinocyte cell line HaCaT 300,493 (Cell Lines Service GmbH). Cells were cultured in DMEM (Dulbecco's modified Eagle's medium, Lonza, Belgium) supplemented with 10 % heat-inactivated fetal bovine serum (FBS) (Gibco, UK) and maintained in T-flasks incubated in a humidified atmosphere with 5 % CO_2 at 37 °C. $5x10^4$ cells were seeded in 24-well plates and incubated until they reached 90 % confluency. Their viability was then examined after 24 h of exposure to different concentrations of BU through mitochondrial function assay using CellTiter Blue (Promega®), following the manufacturer's instructions.

BU immunogenicity was evaluated using the macrophage cell line Raw264.7. Cells were seeded at a density of 1.25×10^4 cells/cm^2 in 12-well plates in in DMEM supplemented with 10 % FBS (HyClone, GE Healthcare, USA). Once cells reached 70 % confluency, Lipopolysaccharide (LPS) (1 μM) and BU were added to the medium and left overnight. The conditioned medium was collected 24 h after stimulation and centrifuged at 15.000xg for 15 min to remove cell debris, and cells from the corresponding wells were counted. Protein levels of TNF-α, IL1β and IL6 were measured by ELISA (R&D System, DuoSet ELISAs TNF-α, IL1β and IL6). Results were normalized to $1x10^6$ cells.

2.6.2. Histological analysis

The tissue samples were sectioned to a thickness of 3 μm and stained with Hematoxylin-Eosin (H&E) for determination of inflammatory cells infiltration (Bisson et al., 2013). Masson's Trichrome (TM) staining was performed according to the manufacturer's protocols and analyzed through bright-field microscopy for the debriding capacity assessment. Specifically, through evaluation of collagen fibers characteristics in the intensity of the blue in Masson's Trichrome (TM) stain. Dark blue represents organized collagen type I fibers while light blue is related with collagen degradation (Kou et al., 2023; Zou et al., 2023). Samples were classified in blind by a specialist pathologist using a score of the collagen degradation level, graded qualitatively from the amount of light blue in the wound area compared with the dark blue in the non-wounding zones of the same tissue section. The score was adapted from a previously reported score (Brunt et al., 1999) and includes values associated with the presence of light blue zones from level 0: absence, level 1: low, level 2: moderated and level 3: high. For vascular area evaluation, immunohistochemical analysis of the sections was performed after deparaffinization and permeabilization with 1 mg/mL digitonin (Sigma-Aldrich) for one hour at room temperature. After that, sections were incubated with BS1-Lectin-Alexa-647 (1:100; Invitrogen) overnight at 4 °C. Nuclei were counterstained with DAPI (Invitrogen). The sections were observed and photographed using an epifluorescence microscope (Leica® Thunder) and then processed with ImageJ analysis software, determining vascular density by the percentage of the area positive for BS1-Lectin-Alexa-647. Values were averaged from 15 images taken in the wound area.

For the analysis of fibroblast proliferation, labeling was performed as reported before (Kawahira, 1999) by incubation with the primary antibody anti-vimentin (Mouse monoclonal V9, Santa Cruz Biotech) and anti-PCNA (Rabbit Polyclonal PCNA, Novus) overnight at 4 °C, and then the sections were labeled and incubated with the secondary antibodies conjugated with Alexa Fluor-598 and Alexa Fluor-488 (Cell Signaling) for 1 h at room temperature, followed by nuclear staining using DAPI (Invitrogen). The sections were observed and photographed using an epifluorescence microscope (Leica® Thunder) to quantify the number of PCNA+nuclei in vimentin+cells and expressed as proliferating cells per field.

2.7. Clinical pilot evaluation

The pilot clinical study was conducted in an outpatient wound care centre in Santiago, Chile. Male and female adults were screened. The study protocol was approved by the Scientific Ethics Committee at Fundación Instituto Nacional de Heridas (Protocol 427605_05112021) and all patients signed the approved informed consent to be included. The study was prospective, randomized, balanced and double-blind. 16 patients were enrolled and randomly assigned into two groups: ulcers treated with BU prototype dressing as the study arm (n = 8), and the control arm treated with Manuka honey dressing established under the trade name Therahoney® sheets (n = 8).

2.7.1. Inclusion and exclusion criteria

Participants were selected according to the following inclusion criteria: patients 60 years or older with venous leg ulcers of 2–15 cm size. Patients were excluded if they had a diagnosis of occlusive arterial disease (ankle-brachial index <0.5); morbid obesity (BMI≥35); cancer treatment in the last year; chronic renal insufficiency (creatinine >2.0 mg); corticosteroid treatment for a period longer than one month; uncontrolled diabetes (glycated haemoglobin over 10 mg/dL); uncontrolled hypertension (blood pressure higher than 140/90 mmHg); or known sensitivity to treatments products or its components.

2.7.2. Outcomes

The main outcome of efficacy was defined as the debriding and antibiofilm effects measured through bacterial load and wound area. For that purpose, bacterial ulcers samples obtained after swabs (ESwab™ Copan) were cultured and quantified through plate counting on CHROMagar Orientation® (Becton Dickinson). The percentage of change between the initial bacterial load at baseline before treatment and that found at day 5 and day 10 of the study interventions were calculated with the following equation (Mouës et al., 2004).

$$\%BacterialChange = \frac{100x(BactLoad\,t - BactLoad0)}{BactLoad0}$$

For the analysis of wound closure, the wound area was measured using a software (EKARE Insight) before the interventions and at visit 1, 3 and 5, and the change in the wound area (% WC) was calculated as reported before (Rötzer et al., 2016).

$$\%WC = \frac{100x(Area0 - Areat)}{Area0}$$

where $Area_0$ is the baseline area measured and $Area_t$ the wound area after treatments.

As part of safety evaluation, pain and/or stinging associated with the dressing applications were evaluated through a clinical score (Labronici et al., 2016).

2.7.3. Study interventions

BU or Honey was applied to the ulcer by soaking a gauze in a blinded setting. In both groups, the dressings were secured with a semi-elastic bandage and rayon fabric as established in the local venous ulcers local clinical protocol. Treatments were applied every 48 h, after visit 1 (V1, day 0) of screening and randomization. In the following visits (V2-V4), dressing change without surgical debridement and ulcer general evaluations were performed up to the end of the study at day 10. At visit 1, 3 and 5 wound size measurement and wound bacterial quantification were performed (Fig. 9).

2.8. Statistical analysis

All data are presented as mean ± standard error of the mean. Statistical analyses were performed using GraphPad Prism (v 8). Normal distribution of data was checked using the D'Agostino-Pearson normality test (alpha = 0.05). One-way ANOVA with Tukey's range test was performed to assess statistical differences between three or more experimental groups. For time-course analysis, two-way ANOVA with Sidak's multiple comparisons test was used. For non-parametric or semi-quantitative analysis, Kruskal-Wallis nonparametric test was applied. Significance was considered at $p < 0.05$. Specific p-values can be found in the figure legends. The ROUT outlier test was applied to clean the data.

3. RESULTS

3.1. BU characterization

Fig. 1 shows the differential scanning calorimetry (DSC) data under three temperature-modifying conditions. The experiments show a thermal transition around 25 °C across all test conditions, indicated by a change in slope on the curves. Notably, when only cooling is applied (Fig. 1C), the observed transition is minor. This subtle shift might be attributed to modifications in the molecular environment, especially since the system starts at an equilibrium state at 25 °C. In Fig. 1A and B, a subsequent change in slope is evident between 100 °C and 121 °C. This temperature range is likely sufficient to disrupt the hydrogen bonds between betaine and urea. Upon cooling, both curves show another shift in slope around −25 °C. Notably, this transition does not appear when the system is initially cooled, as seen in Fig. 1C, which shows the cooling curve from 25 °C to −75 °C. For this reason, no significant change in slope is observed in curve C. In contrast, in curves A and B, freezing

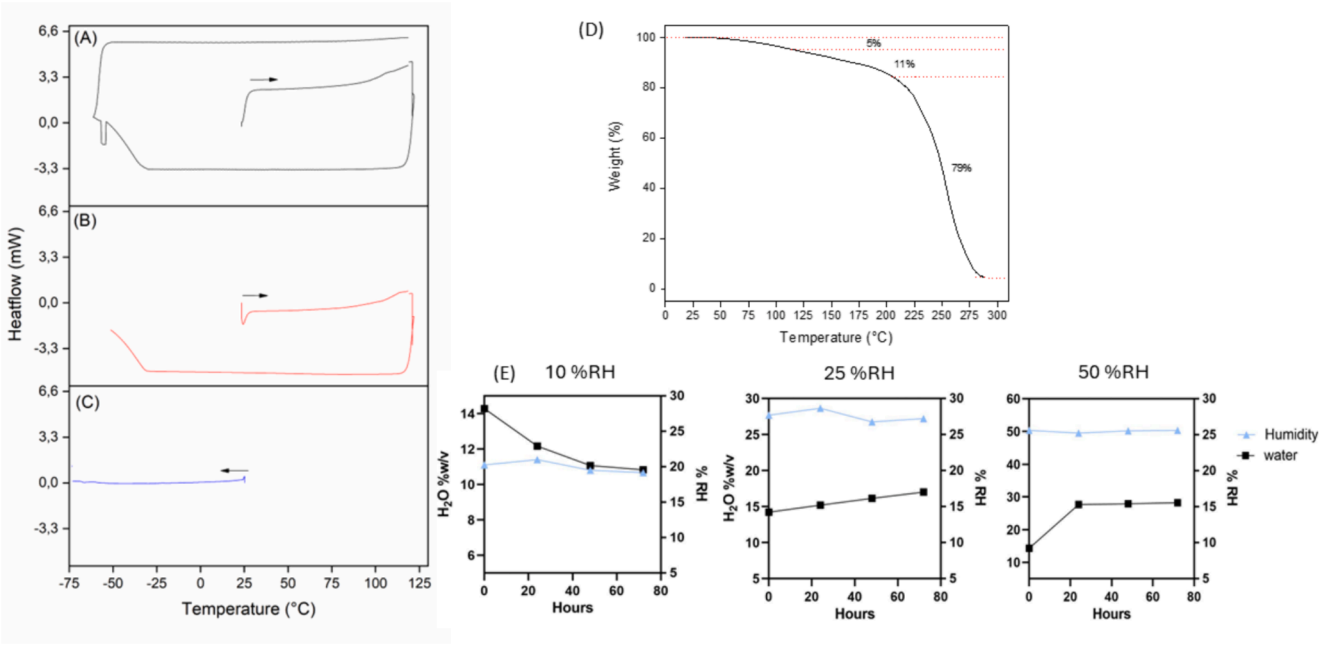

Fig. 1. Physicochemical characterization of BU. Differential Scanning Calorimetry (DSC) of BU **(A)** Sequence of heating, cooling, and reheating. **(B)** Sequence of heating followed by cooling. **(C)** Cooling only. **(D)** Thermogravimetric analysis (TGA) of BU. Data obtained from 25 °C to 290 °C. **(E)** Hygroscopicity. Water content of BU in different percent relative humidity (%RH) environments. Data are shown as mean ± SEM, n = 3.

occurs when the BU structure is no longer present. When reheated, as shown in Fig. 1A, no noticeable transitions are evident. This indicates that the process is not reversible, and the supramolecular structure undergoes changes during the analysis performed under the DSC measurement conditions. Throughout the study temperature range, there is no appreciable variation in the curve, maintaining the heat flux close to zero and indicating the absence of endo- and exothermic phenomena.

Fig. 1D shows the thermogravimetry analysis (TGA) from 25 °C to 290 °C obtained for the BU sample. Three considerable mass losses are observed. The first may be associated with the dehydration process of water in BU. Subsequently, a second drop in the slope is observed above 100 °C, which can be attributed to a preliminary decomposition process of urea, considering that its decomposition temperature is close to 160 °C (Zhu et al., 2021). Around 200 °C, a drastic mass loss is observed, which is related to the decomposition of both components and the loss of the BU structure. Although betaine has a higher decomposition temperature after melting from its solid state, around 300 °C (Sánchez et al., 2019).

In relation with hygroscopicity, the results in Figure E, showed that when the BU formula with a water content of 14.2±0.004 %w/w is left under humidity environment of 25 % RH, it progressively hydrates leading to water content of: 15.2±0.004 %, 16.3±0.003 % and 17.02 ±0.003 %. In the same sense, at high relative humidity of 50 % RH BU rapidly hydrates, and before 20 h it reaches a water content of 28.2 ± 0.14 %w/w. Conversely, under 10 % RH, BU dehydrates progressively obtaining the following water contents: 13.5±0.005 %, 12.7±0.003 % and 11.5±0.2 % w/w. The low water content obtained at the end of the 3 days experiment under low humidity resulted in the solidification of the mixture.

3.2. BU debriding in vitro effect

Ultraviolet spectroscopy was utilized to evaluate the BU debriding effects on the artificial slough over time. Results showed that BU induces

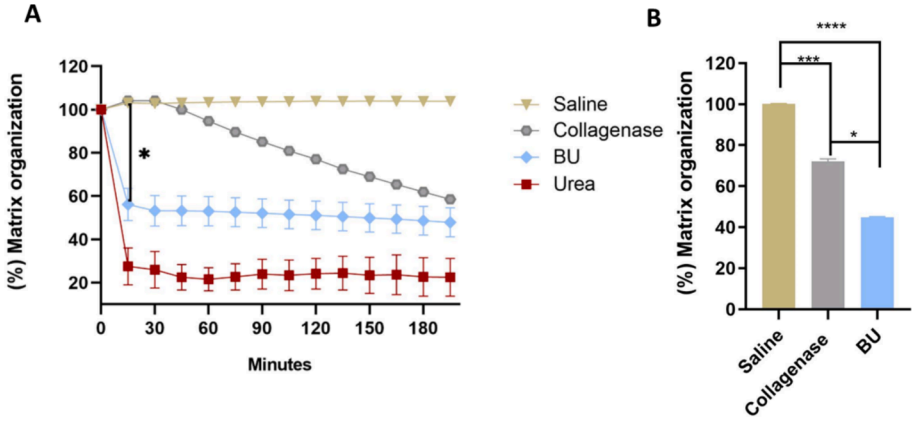

Fig. 2. Debridement effect of BU on an artificial wound slough model. Disorganization of the matrix was analyzed through UV absorbance at 350 nm. **(A)** Kinetic slough matrix disorganization after 3 h treatments exposure. *P <0.05 two-way ANOVA. **(B)** Quantification of endpoint effect of BU and collagenase on the slough matrix disorganization. Data are expressed as percentage of total absorbance of the scar matrix treated with saline. Data are showed as mean ± SEM, n = 3, *P<0.05; ***P <0.001 one-way ANOVA.

a rapid and robust matrix disorganization, evidenced by a decrease in its light absorbance capacity (Fig. 2A). BU application significantly lowers the absorbance, leaving 56±3.5 % of the original structure after 15 min compared to the artificial slough treated with saline, with no further changes until the end of the experiment (Fig. 2A and 2B). By contrast, collagenase showed a more delayed effect, starting to act on the matrix after 1 h of incubation, decreasing the absorbance progressively and leaving 62±0.5 % of the slough at the end of the experiment (Fig. 2A and 2B). The reduction in matrix organization induced by BU, analysed though ultraviolet absorbance of the matrix, was significantly higher than that induced by collagenase but moderated compared to the potent effect of urea solution, which leaves only 22±5.6 % of the initial matrix structure. Saline, on the other hand, had no effect on the organization of the artificial slough. The higher level of matrix disassembly induced by BU in comparison to collagenase observed by this method may be related to the higher separation of the protein chains induced by the high hygroscopicity of BU, leaving a looser matrix with less light absorbance capacity.

Another indicator for matrix disorganization is the leaching of proteins from the artificial scar. For measure that variable, fluorescence-labeled elastin was incorporated into the artificial slough, and leaching was quantified by measuring fluorescence intensity over time. Fig. 3A shows that BU significantly promotes elastin detachment from the matrix after 30 min of incubation compared to saline-treated artificial sloughs, reaching 67±2.9 % of the collagenase total debridement capacity in 24 h. Collagenase had a significantly more pronounced effect on elastin release than BU (Fig. 3A). This result is associated with the erosion or breakdown effect of the treatments, which was more pronounced due to the proteolytic characteristics of collagenase, inducing a higher degree of elastin elusion. Nevertheless, although to a lesser degree, BU also induces the leaching of proteins, suggesting that the destructuration induced is able to cause a significant degree of erosion.

There was only minor fluorescent elastin released in the presence of saline, with the main increase observed in the first 30 min of incubation (21±0.4 %), followed by a minor increase to 28.4±3.5 % until 24 h.

Also, Fig. 3B shows that BU causes a significant swelling of the proteinaceous artificial matrix over time, and the same effects can be observed when BU was evaluated on a clinically relevant matrix obtained directly from patients with chronic wounds (Fig. 3C). In both cases, BU had a pronounced effect over saline on swelling reaching a 255 ±22 % swelling increase after 10 min and 855±34 % swelling increase after 24 h of BU incubation for the artificial sloughs (Fig. 3B). For the clinical slough samples, BU significantly increased swelling, reaching a 422±36 % increase after 10 min compared to the 137±5 % increase of swelling induced by saline incubation (Fig. 3C). Notice that in clinical samples treated with BU, it was not possible to perform the mass measurements after 120 min of BU incubation due to the complete disintegration of the samples.

3.3. BU antibiofilm in vitro effect

The artificial slough model represents a solid and fibrous proteinaceous support for bacteria to form biofilms, similar to clinical wound colonization (Price et al., 2016). Fig. 4 shows the antibiofilm activity of the treatments against a mixed biofilm of *P. aeruginosa* and *S. aureus* with the following bacterial viability counts: i) for 24 h biofilms treated with: saline $1.0x10^8$±$1.6x10^5$, BU $2.2x10^6$±$8.0x10^5$, PHMB-Betaine $2.2x10^7$±3.2 $x10^6$ and Honey $3.6x10^8$±$7.6x10^7$ (Fig. 4A); ii) for 48-hour biofilms treated with: saline $4.0x10^8$±$1.6x10^7$, BU $1.0x10^8$±$1.7x10^7$, PHMB-betaine $8.7x10^7$±$2.2x10^6$, and Honey $2.1x10^8$±$3.9x10^7$ (Fig. 4B); iii) for 72-hour biofilms treated with: saline $1.2x10^8$±$2.1x10^7$, BU $6.4x10^7$±$7.8x10^6$, PHMB-betaine $7.5x10^7$±$1.0x10^7$ and Honey $2.3x10^8$±$3.6x10^7$ (Fig. 4C). These results indicate that BU has a strong antibiofilm effect in 24-hour and 48-hour biofilms, which was comparable to the antibiofilm effect induced by the antiseptic PHMB-betaine, while Honey has no antibiofilm effect or even promotes bacterial growth.

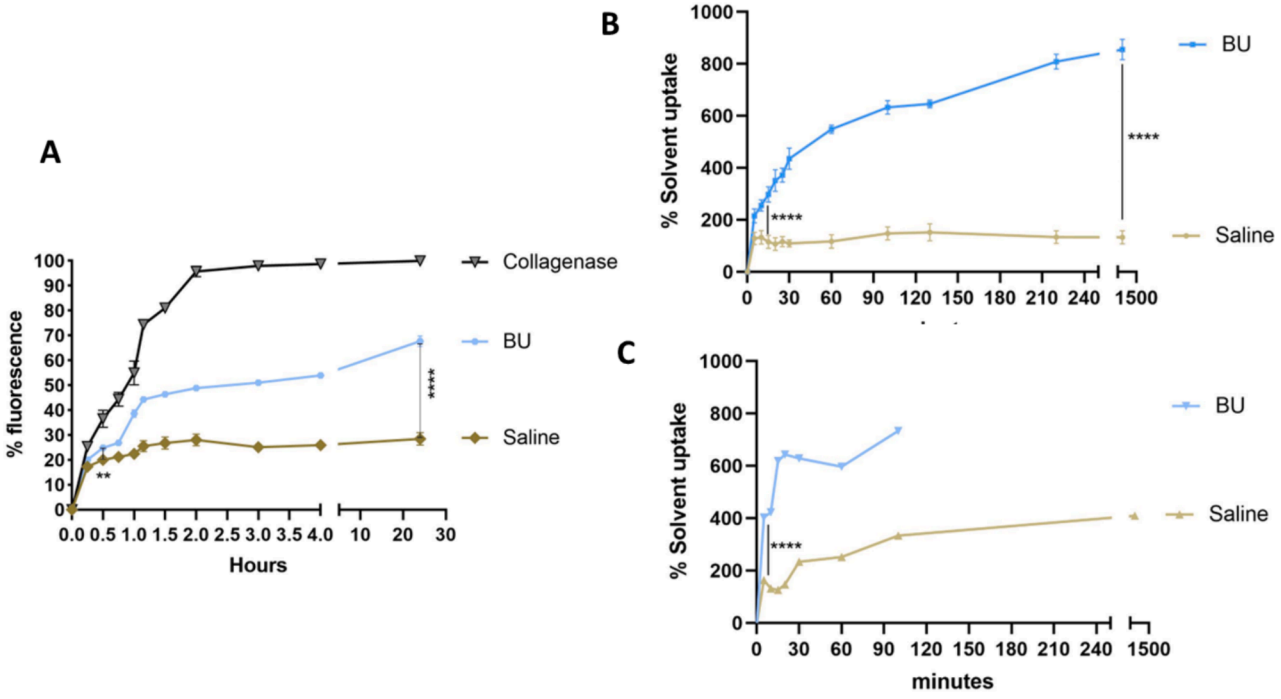

Fig. 3. Debridement effect of BU on an artificial slough model. (A) Kinetic evaluation of the release of labelled elastin after treatments. Slough matrix debridement effect analysed through percentage of florescence (Ex 360 nm Em 444 m). (B) Kinetic evaluation of solvent uptake as surrogate of swelling of the artificial slough. (C) Kinetic evaluation of solvent uptake as surrogate of swelling of the clinical slough samples. Data are displayed as mean ± SEM, n = 3 ****P <0.0001 two-way ANOVA.

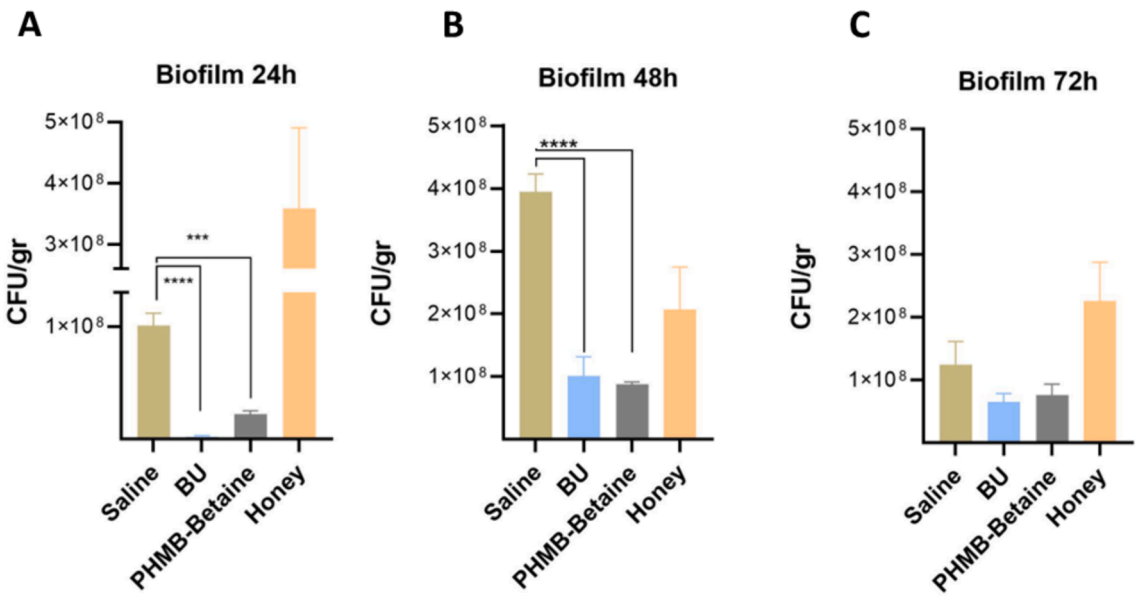

Fig. 4. Antibacterial effect of BU on a biofilm cultured on the artificial slough. Viable bacterial count of mixed biofilms of *S. aureus* and *P. aeruginosa* of 24 h **(A)**, 48 h **(B)** and 72 h **(C)**, after 24 h treatment. Data are shown as mean ± SEM, n = 3, ***P <0.01, ****P <0.001 one-way ANOVA.

3.4. BU antibiofilm ex vivo effect

The *ex vivo* wound-inoculated model represents a realistic solid substrate for bacteria to form biofilms. Fig. 5 shows the antibiofilm activity of the treatments against a mixed biofilm of *P. aeruginosa* and *S. aureus* with the following bacterial viability counts: i) for 24 h biofilms treated with: saline $2.9x10^8 \pm 2.9x10^7$, BU $6.5x10^7 \pm 8.0x10^6$, PHMB-Betaine $3.3\ x10^8 \pm 2.3\ x10^7$ and Honey $3.4\ x10^8 \pm 7.6\ x10^7$ (Fig. 5A); ii) for 48 h biofilms treated with: saline $3.7x10^8 \pm 1.0x10^8$, BU $2.7\ x10^7 \pm 9.5x10^6$, PHMB-betaine $1.7x10^8 \pm 5.9x10^6$ and Honey $3.8\ x10^8 \pm 3.4\ x10^7$ (Fig. 5B); iii) for 72 h biofilms treated with: saline $2.8x10^8 \pm 6.2x10^7$, BU $8.6x10^7 \pm 9.4x10^6$, PHMB-Betaine $2.4x10^8 \pm 2.1x10^7$ and Honey $1.7x10^8 \pm 1.9x10^7$ (Fig. 5C). These results indicate that BU, as in the case of the artificial slough, also has a strong antibiofilm effect in the *ex vivo* wound inoculated model that could be evidenced in 24-hour, 48-hour and 72-hour biofilms. However, in this model, BU had a stronger effect compared to the antibiofilm effect induced by the antiseptic PHMB-betaine. Conversely, Honey has no antibiofilm effect in this model.

3.5. BU antibiofilm and debriding effect in in vivo murine model

A valuable approach for assessing antibiofilm activity in a scenario closer to a clinical wound situation is using an *in vivo* murine model. Diabetes mellitus was induced in these animals by streptozotocin administration since this model resembles the wound healing and biofilm colonization complications observed in humans (Krishnan et al., 2018; Ezquer et al., 2015). Thirteen days after diabetes induction, a wound was generated in the neck of the animals and inoculated with *P. aeruginosa* and *S. aureus*. Fig. 6A presents the results of viable bacteria

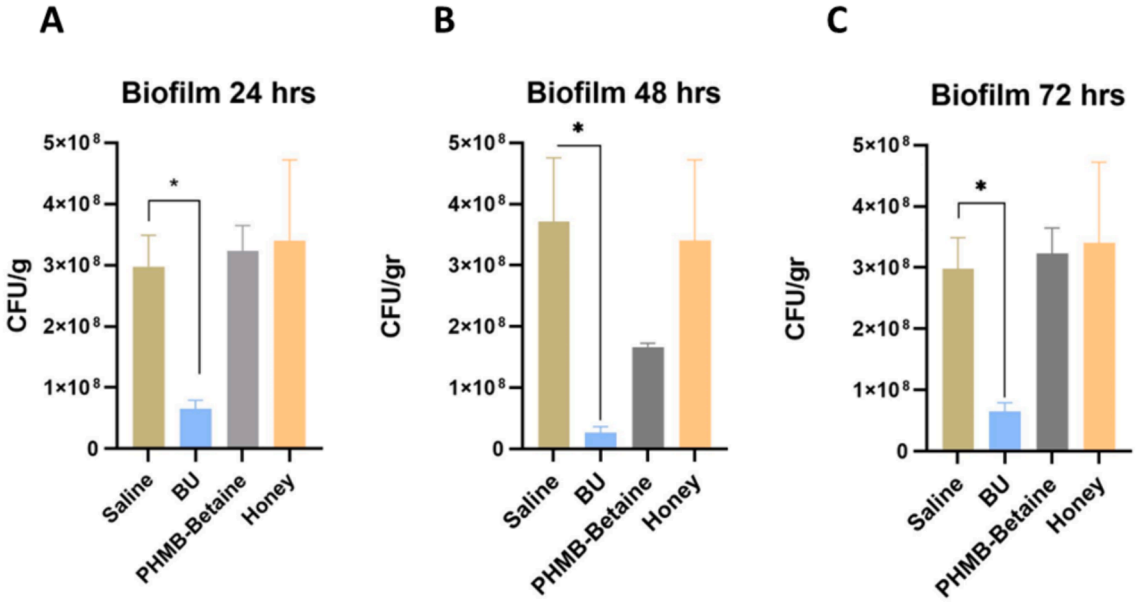

Fig. 5. Antibacterial effect of BU on biofilms cultured on human skin explants. Viable bacterial count of mixed biofilms of *S.aureus* and *P. aeruginosa* at 24 h **(A)**, 48 h **(B)** and 72 h **(C),** after 24 h treatment. Data are shown as mean ± SEM, n = 3. *P <0.05 one-way ANOVA.

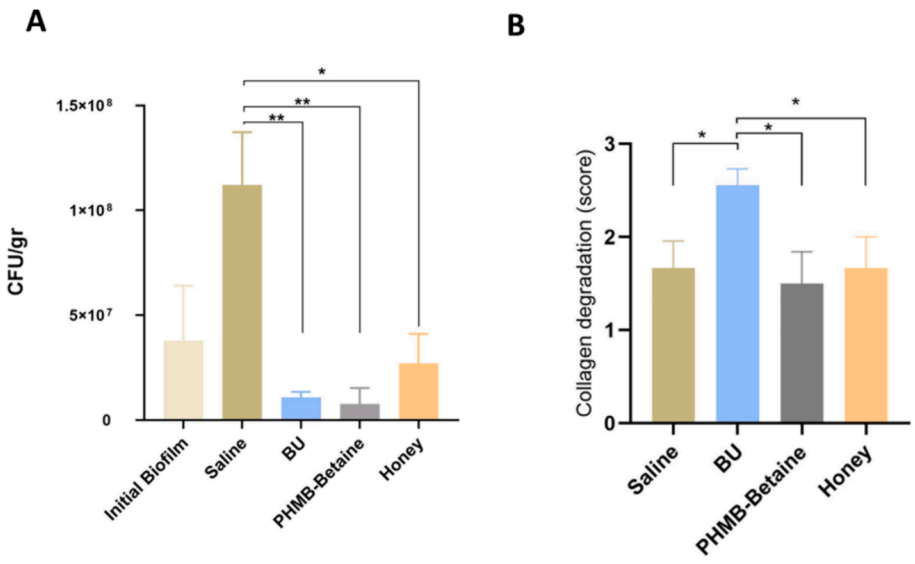

Fig. 6. Antibiofilm and debriding *in vivo* effects of BU. (A) Viable bacterial count in wounds after treatments. Data are shown as mean ± SEM, n = 10 *p <0.05, **p <0.01 one-way ANOVA. **(B)** Quantification of collagen degradation through a score based on the collagen fibres in the Masson staining. Data are shown as mean ± SEM, n = 10. *p <0.05 Kruskal-Wallis.

counts following treatment applications, every 48-hour. The bacterial viable count was in the saline group $1.1x10^8 \pm 3.8x10^7$, in the BU group $1.1x10^7 \pm 4.0x10^6$, in the PHMB-Betaine group $7.7x10^6 \pm 4.6x10^6$, and in the Honey group $2.7x10^7 \pm 1.0x10^7$, showing that the three therapeutic treatments evaluated had similar *in vivo* antibiofilm effects.

Fig. 6B depicts the evaluation of the debriding effect through analysis of animal tissue sections using Masson Trichrome staining. The effect was evaluated through a score of the blue stain intensity of the collagen fibers, associated with the collagen degradation level (Chen et al., 2017; El-Sayed et al., 2024). Results indicated that BU was the only treatment able o significantly increase collagen degradation.

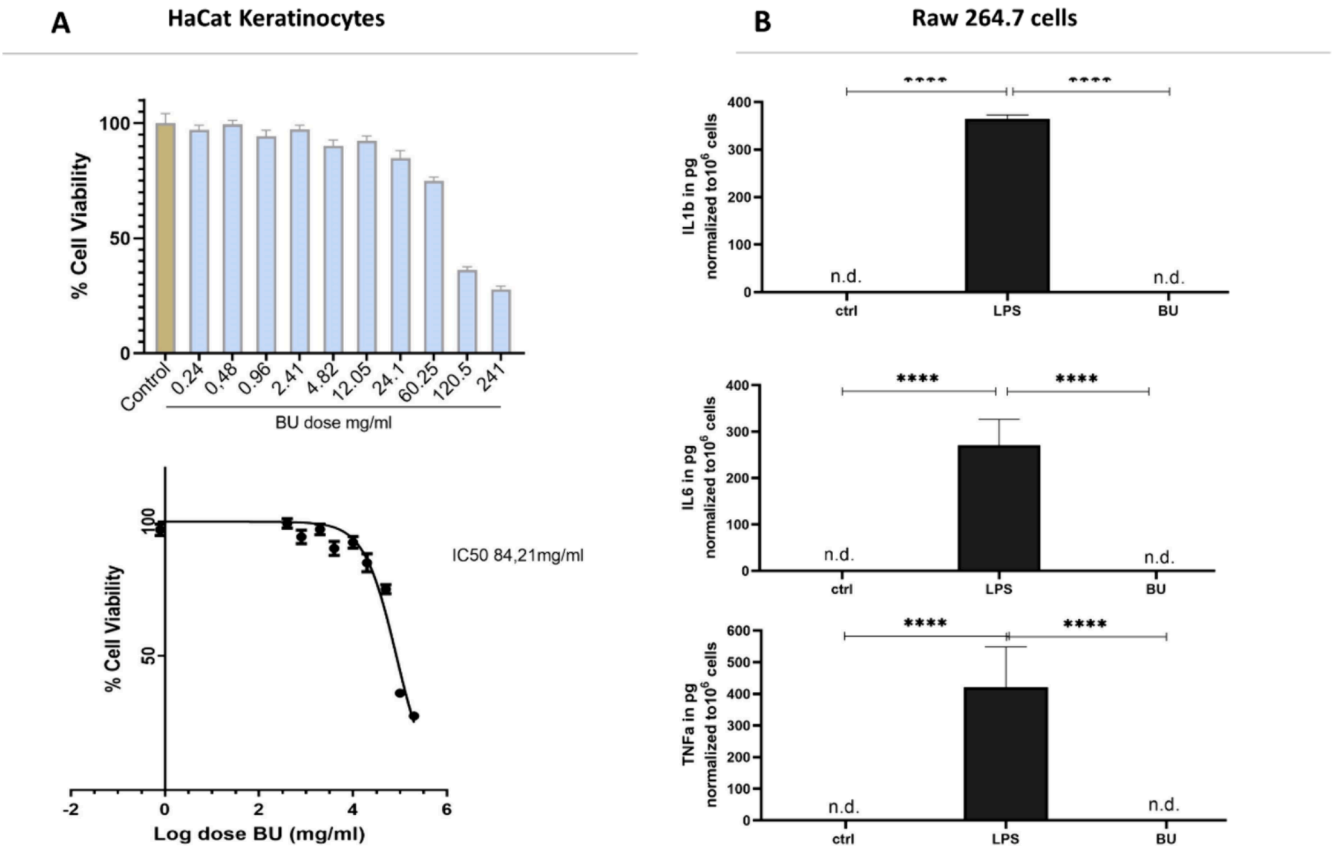

Fig. 7. Evaluation of BU cytotoxicity and immunogenicity. (A) Viability of HaCaT cells after 24 h of BU exposure assessed by mitochondrial activity evaluation and determination of the IC_{50} **(B)** Determination of secretion of the pro-inflammatory cytokines IL-1β, IL-6 and TNF α by RAW 264.7 cells measured by ELISA and normalized to $1x10^6$ cells. Data are shown as mean±SEM, n = 3, ****p <0.0001 one-way ANOVA.

3.6. BU preclinical in vitro and in vivo safety evaluation

Safety evaluations of BU were performed through cytotoxicity tests and histology analysis in the murine tissue samples. Cytotoxicity assessment on HaCaT cell viability allowed the calculation of BU IC_{50}, giving a value of 84.21 mg/mL (Fig. 7A). Additionally, the immunogenicity experiment in raw cells indicated that incubation for 24 h with BU did not induce pro-inflammatory cytokine secretion while the incubation of these cells with LPS, a classical pro-inflammatory stimulus, induced a significant increase in TNFα, IL6 and IL1β secretion (Fig. 7B).

For *in vivo* safety evaluation of BU, wound tissue sections from the different experimental groups were evaluated, focusing on two central variables that could affect tissue regeneration processes: vascularity (BS1-Lectin staining) and fibroblast proliferation (PCNA/Vimentin) status through histological evaluation. Data indicated that there were no significant changes in these parameters across the different experimental groups (Fig. 8A and B). Moreover, the inflammatory status of the wound tissues was also evaluated, and although BU treatment induced a lower level of polymorphonuclear neutrophils (PMNs) and lymphocyte infiltration (CD3), there were no significant difference between experimental groups, indicating that BU treatment does not induce toxic effects in the treated skin.

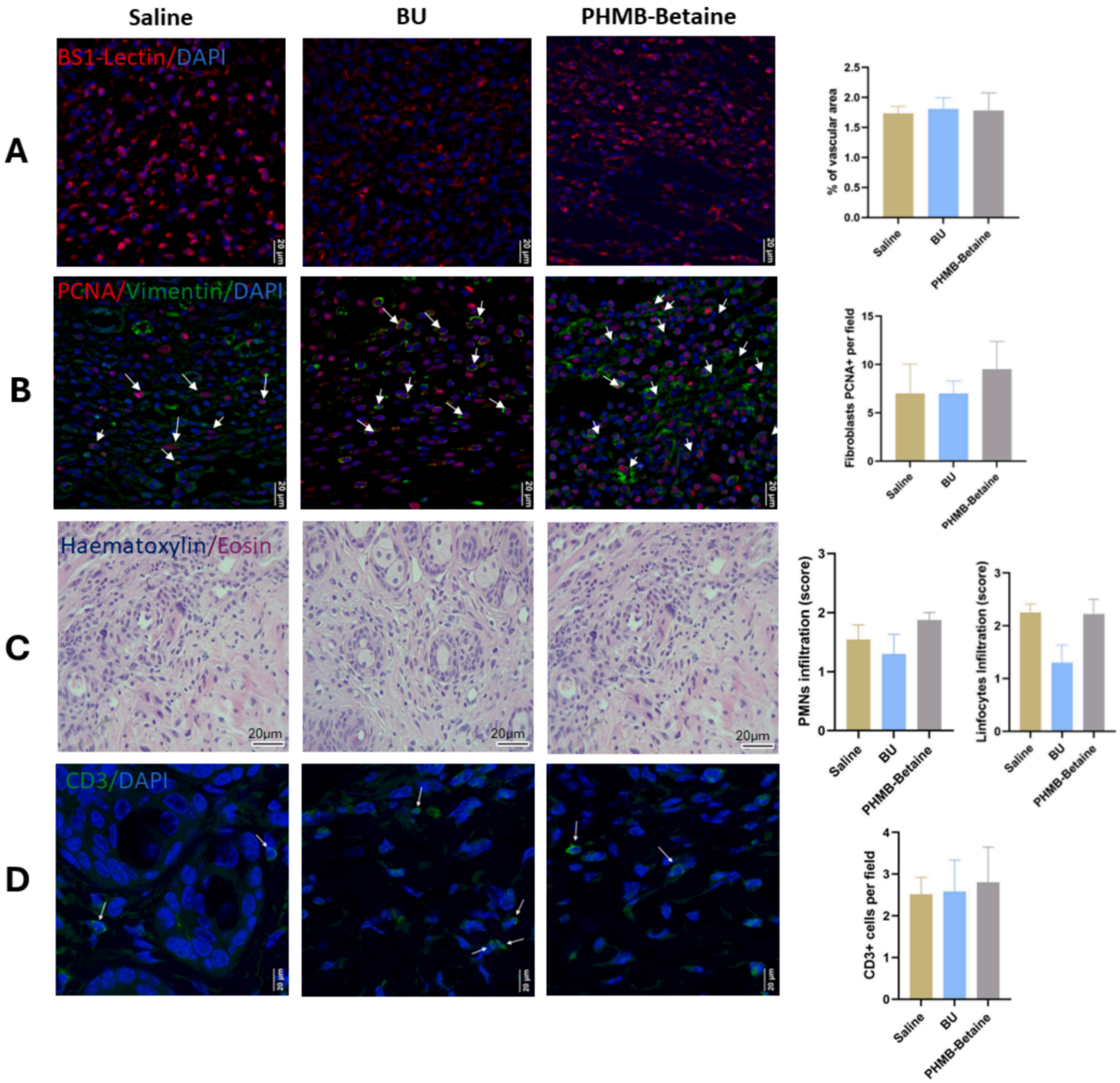

Fig. 8. Preclinical BU safety evaluation through histological analysis. (A) Quantification of vascularity through fluorescence analysis of the area with positive tinction for Lectin-BS-1 marker. **(B)** Quantification of fibroblast proliferation through fluorescence analysis of the nuclear protein marker PCNA, a marker of the proliferative state of fibroblasts (detected by anti-vimentin immunoreactivity) showed by arrows. **(C)** Quantification of polymorphonuclear (PMN) and total lymphocyte infiltration analysed by light microscopy in sections staining with Haematoxylin-Eosin, scored by a specialized pathologist. **(D)** Quantification of T cells infiltration by immuno-analysis with primary antibody anti CD3. Scale-bar indicate 20 µm. Data are shown as mean ± SEM, n = 5.

3.7. BU pilot clinical evaluation

Finally, to evaluate the therapeutic properties of BU in clinical wounds, sixteen patients with venous leg ulcers were randomized, eight in the study arm of BU and eight in the comparator product Manuka honey (Therahoney™) study arm. All patients adhered to the study visits and completed the follow-up schedule, schemed in Fig. 9A.

Fig. 9B shows that at day 5, the microbial load in the wounds of patients treated with BU exhibited a reduction of 82±8.3 % compared to their initial microbial load. In contrast, patients treated with Honey showed a large variation in their data, with a considerable increase in the ulcer bacterial load of 383±178 % compared to their initial state. When comparing both experimental groups, there was a statistically significant difference in the bacterial load change ($p < 0.05$). At day 10, patients treated with BU showed a bacterial load reduction of 48±27 %, while patients treated with Honey showed a significant increase in bacterial load of 2508±1584 %. The comparison between experimental groups also showed a statistically significant difference ($p < 0.05$) (Fig. 9B).

Finally, the other outcome, the ulcer areas was quantified. In Fig. 9C, it can be observed that on the fifth day of the study, patients treated with BU had an 8.8±11 % wound area reduction, while patients treated with Honey reached a 20±4.9 % wound area reduction. However, on day 10, patients treated with BU showed a wound area reduction of 36±9.7 %, while patients treated with Honey had a 19±7.7 % wound area reduction. This indicates that BU can significantly reduce bacterial load and improve wound closure in clinical ulcers. There was no difference in pain levels between the treatment groups (data no shown).

4. Discussion

4.1. BU has a dynamic microstructure

The dynamic modification of the hydrogen bonding interactions associated with the changes in temperatures observed through the transitions during DSC experiments has been previously reported for NADESs (Abranches et al., 2020; Olivares et al., 2022; Mecham and Birk, 2013). Additionally, the hypothesis of betaine modulating the chaotropic nature of urea was supported by this dynamic nature of the hydrogen bonding network in BU. This dynamism was also analysed by NMR in previous studies (Olivares et al., 2018), which reported that the freedom of the individual molecules is also modulated by the composition of the NADES. On the other hand, the potent antibiofilm effect might be a property of the microstructure of BU, characterized by its hyperosmolarity and high hygroscopicity, as this effect is not observed when its components are used separately (Olivares et al., 2022).

The DSC analysis supports the hypothesis that the hydrogen bonds break at elevated temperatures, leading to the loss of the structure typical of a deep eutectic liquid. On the other hand, when BU is only cooling, the hydrogen bonds do not break; instead, the cooling process aids their formation, leading to freezing.

The TGA measurements indicates the stability of BU is different that the individual components. This phenomenon could be due to the aggregation state in a deep eutectic system, previously described for other NADESs (Chen et al., 2018).

BU exhibits a rapid disorganization effect on proteinaceous matrix.

The artificial slough is a valid model frequently applied during in vitro cutaneous tissue studies because it allows the assembly of main extracellular proteins similarly as observed *in vivo* (Mecham and Birk,

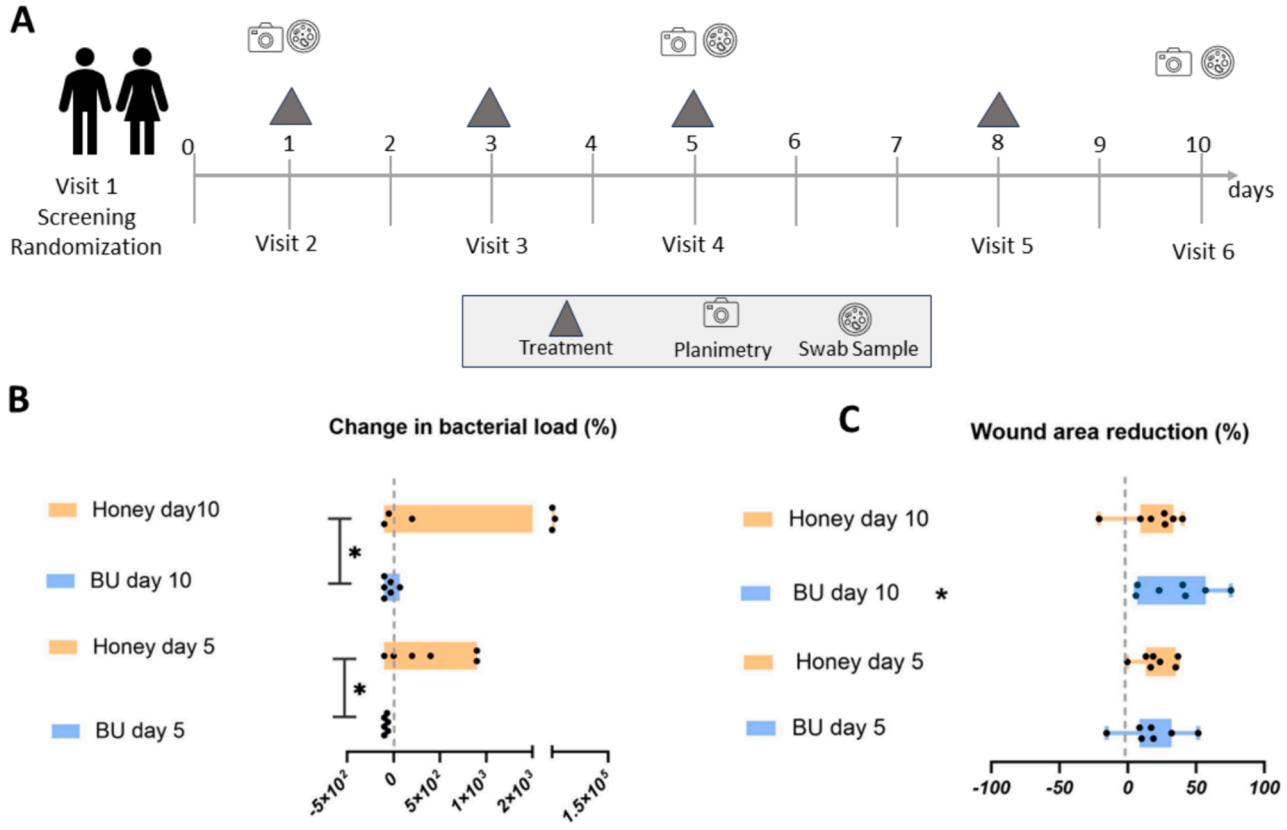

Fig. 9. Pilot clinical results comparing BU and Honey. (A) Study design and outcomes measurements from the baseline individual status and their status at middle (day 5) and at the end of the study (day 10). **(B)** Quantification of ulcer bacterial load as a surrogate of the debriding and antibiofilm effects. Data are shown as mean and ± SEM of 8 ulcers per experimental arm. *P <0.05 Kruskall-Wallis. **(C)** Quantification of wound area reduction. Data are shown as mean and ± SEM of 8 ulcers per experimental arm. *P <0.05 one sample *t*-test.

2013; Forgacs et al., 2003). The kinetically absorbance measurements are directly related to the density of the artificial slough matrix (Stuart and Panitch, 2008). From the results obtained, it is noticeable that BU modifies the slough structure suggesting that the diminishing in absorbance is caused by an increased in the pore sizes of the matrix. This effect is almost instantaneous, and it is maintained until the end of the assessment, indicating that BU induces significant disorganization of the matrix.

The hygroscopicity of BU observed in high humidity environments could be related to the observed disorganization of the proteinaceous slough matrix. There is a remarked avidity of the BU constituents to form hydrogen bonding, which forces the surrounding water molecules to be included into the BU structure. At the same time, based on the hydrogel nature of the slough matrix, a strong swelling with BU molecules getting between the polymeric fibrils occurs as observed from the swelling experiment (Wang et al., 2019). Additionally, the changes generated by BU in the matrix density also induce the leaching of proteins, suggesting that the de-structuration mechanism also causes a significant degree of erosion. This effect is typically related to the mass loss of hydrogels-type matrices as a mechanism of destabilization (Woodard and Grunlan, 2018). (Wijayapala et al., 2017). In general, the probable mechanism of matrix disorganization is based on dehydration and simultaneous incorporation of BU between the protein fibrils. However, the chaotropic effect of urea on proteins has been extensively reported (Franks, 1995), thus it is expected that the disorganization effect is driven by this urea property. However, in BU formula, urea is strongly compromised with betaine, leading to a modulated chaotropic effect as it was previously reported (Stasiulewicz et al., 2021; Ganguly et al., 2022). Thus, explaining the attenuated effect of BU compared with urea solution of the same concentration on the debriding capacity. This is specially desired in the wound field treatments, where reaching a balance between debridement of dirty and devitalized tissues and preserving the regeneration in wound beds is mandatory (Rajhathy et al., 2021).

4.2. BU reduces bacterial biofilm

The artificial slough gave us the opportunity to culture the biofilm on protein fibers, allowing the formation of a dense bacterial community within 24 h. In this model, some previously described effects were observed, such as the different maturation stages of biofilms, which include the periodic (partial) dispersal and shedding of planktonic bacteria. Restructuration, dispersal or shedding of bacteria is induced by several factors, including nutrient availability, which has been described for *P. aeruginosa* (Sauer et al., 2004) and *S. aureus* (Moormeier and Bayles, 2017). These biofilm restructuring effects could explain the variations in bacterial count over time observed in the biofilm of the control group. A pronounced and statistically significant antibiofilm effect of BU was observed at this early maturity stage, which then decreased as the biofilm became more tolerant up to 72 h, similar to the PHMB-Betaine treated group. In contrast, Honey treatment increased the bacterial count at the three-time evaluated. Biofilm tolerance is known to be more related with other mechanism different from increase in bacterial counts, which can explain why the bacterial count was stable in the control group across the different time intervals (Stewart and Costerton, 2001). In this sense, exopolysaccharide can modulate its characteristic based on the bacterial growing-feeding conditions (Wu et al., 2012). Probably, in the artificial slough model, with fibers highly embedded by the culture media, the exopolysaccharide becomes denser across the three-time intervals, helping to prevent bacterial death.

The organotypic bacterial colonized model obtained through the biofilm culture in human explants, offer the dermal structure, with a denser tissue fibre compared to the artificial slough. Under these conditions BU induced a significant decrease in the bacterial viability across all three-biofilm maturity stage studied. In contrast PHMB-Betaine and Honey did not show antibiofilm results. Probably, in the human skin explant, the biofilm grows more intricated into the denser extracellular matrix, thus less accessible to the superficial contact of the evaluated products than in the artificial model, with less dense protein fibres. However, due to the debriding capability that BU possess, it allows for higher penetration and thus achieved a comparatively superior antibiofilm effect in the three-time intervals.

The wound model colonized with biofilm in diabetic mice represents a pre-clinical model close to clinical scenarios of chronic wounds. The general physiological state in these animals promotes the formation of biofilms that are difficult to eradicate because of the impaired action of the immune system among others worsen regeneration conditions (Ezquer et al., 2016; Marhoffer et al., 1992). In this study, the initial bacterial load inoculated in the wound was able to form a 48-hour mature biofilm, which persisted despite frequent saline cleaning interventions in the control group. In this model, BU produced a logarithmic reduction in the bacterial load compared to the control group. This effect, which coexist with the immune system fighting bacteria, was similar to that observed with the application of PHMB-Betaine and Honey.

In the literature, the debridement effects are mostly evaluated through the reduction of bacterial load as a surrogate measurement of this outcome (Wilkinson et al., 2016; Kataoka et al., 2021). In this study, the semiquantitative observation of the quality of collagen fibres in the wound area support the fact that BU modifies the density of type I collagen present in the wound bed, underlying the direct debridement effect of BU.

Finally, the antibiofilm effect evaluated during the clinical trial was compared to Honey. This choice was due to its composition characteristics, since in clinical practice Honey has reported evidence of both, debriding and antibiofilm attributes (Jull et al., 2015; Yilmaz and Aygin, 2020). The bacterial load data showed a significant increase at 5 and 10 days in the Honey arm of the evaluation, whereas in patients treated with BU, the bacterial load remained stable over the 10 days in relation to their baseline state and was significantly reduced compared to Honey treatment. Some studies with Honey indicate that a bacteriostatic effect occurs on patients' ulcers under short periods of treatment (Wang et al., 2019). This observation is based on the bacterial nutritive effects of sugars in Honey. Additionally, the wound area results show that the evaluation at 5 days was better in Honey group, but at 10 days, BU significantly reduced the wound area compared to the baseline condition. In the Honey group, there was not a significant wound area reduction, probably related to the increase in bacterial load.

BU anti-biofilm capacity observed across the different models are possible related to similar mechanisms underlying the observations on the disorganization of the artificial slough matrix, which is the water and protein modification caused by the hygroscopicity and the chaotropic effect of BU on the biofilm structure.

Bacteria living in biofilms are held together by a polymeric matrix that keeps them in communication and protects them from the effects of antibiotics, ultraviolet light, and the immune system, making them highly resilient forms of life (Bjarnsholt et al., 2018). Water channels in biofilms have been described as a vital component for this communication and the maintenance of community viability (Quan et al., 2022). Thus, affecting the biofilm's water-retention capacity is a good target to disassemble it (Quan et al., 2022). Many reports have shown that products physically affecting the biofilm structure are more effective in critically colonized wounds, achieving strong healing results with the same kinetics as many potent antiseptics, but with fewer adverse effects (Jull et al., 2015; Carter et al., 2016). Accordingly, we hypothesize that the anti-biofilm capacity of BU observed across the different models is possible related to these mechanisms. This could be achieved through the disorganization of the artificial slough matrix, by the water uptake and protein modification caused by the high hygroscopicity and the chaotropic effect of BU on the biofilm structure. Importantly, the antibiofilm effect is not observed when both components (betaine and urea) are evaluated separately (Olivares et al., 2022), suggesting that the supramolecular structure of BU is responsible for the physical antibiofilm

effect.

In this work, preclinical results of BU, a non-biocidal formulation, demonstrate reduction of biofilm bacterial viability to the same extent as the commercial biocidal formulation PHMB-Betaine, whose components are reported to have effective broad-spectrum antimicrobial properties (Stewart and Costerton, 2001; Hengzhuang et al., 2011). Moreover, in the relevant clinical environment BU, was more effective in controlling the bacterial load than medical honey, leading to better healing rates. During the clinical evaluation, the pain assessment was good in both groups, indicating that BU application had a similar tolerance to Honey.

4.3. BU is a biocompatible formulation

Before conducting the *in vivo* murine study, BU's cytotoxicity was evaluated in keratinocytes, and the calculated IC_{50} was in the molar concentration range. This result is similar to the IC_{50} reported in a previous work in human fibroblasts (Olivares et al., 2018); both indices fall into the non-toxic category of materials. Additionally, as part of the biocompatibility assessment, BU's potential to generate an immunogenic response in murine monocytes, which could be an adverse and confounding factor in the animal evaluation was tested. BU did not induce secretion of proinflammatory cytokines compared to the LPS stimulus. Then, the murine *in vivo* biocompatibility of BU conducted on critical variables, support the non-toxicity and abled the advancement to the execution of broader clinical evaluation.

5. Conclusion

Recognizing the differences between bacteria growing in biofilms and planktonic, has explained why it is more challenging to combat chronic colonization characterized by biofilms and have been promoting the application of new non-biocide strategies for debridement.

The hypotheses that it is possible to achieve a moderate debriding effect, suitable for application in sub-epidermic tissues in wounds, together with the antibiofilm capacity derived from the unique supramolecular structure observed in a NADES formulation, was increasingly evaluated through various relevant in vitro and *in vivo* models, generating preclinical and clinical evidence of these characteristics. In this context BU could represent a simple topical, non-biocide anti-biofilm and debridement biomaterial. Thus, representing a valid and highly desirable therapeutic option.

CRediT authorship contribution statement

Christina MAP Schuh: Writing – review & editing, Methodology, Formal analysis, Data curation. **Fernando Ezquer:** Writing – review & editing, Methodology, Formal analysis, Data curation. **Sigde Mamani:** Writing – review & editing, Methodology, Data curation. **Paola R. Campodónico:** Writing – review & editing, Data curation. **Constanza Cárcamo:** Writing – review & editing, Data curation. **Fabián Martinez-Gómez:** Writing – review & editing, Data curation. **Isabel Aburto:** Writing – review & editing, Methodology, Data curation. **Marcelo Ezquer:** Writing – review & editing, Data curation. **Bernardo Morales:** Writing – review & editing, Data curation. **Belén Olivares:** Writing – review & editing, Methodology, Funding acquisition, Formal analysis, Data curation, Conceptualization.

Declaration of competing interest

The authors declare that they have no known competing financial interests or personal relationships that could have appeared to influence the work reported in this paper.

Data availability

Data will be made available on request.

Acknowledgements

This work was supported by the Agencia Nacional de Investigación y Desarrollo (ANID) [FONDEF ID 21|10053] to Belen Olivares.

References

Abranches, D.O., Silva, L.P., Martins, M.A.R., Pinho, S.P., Coutinho, J.A.P., 2020. Understanding the formation of deep eutectic solvents: Betaine as a universal hydrogen bond acceptor. ChemSusChem 13 (18), 4916–4921.
Aroso, I.M., Paiva, A., Reis, R.L., Duarte, A.R.C., 2017. Natural deep eutectic solvents from choline chloride and betaine–Physicochemical properties. J. Mol. Liq. 241, 654–661.
Bisson, J.F., Hidalgo-Lucas, S., Bouschbacher, M., Thomassin, L., 2013. Effects of TLC-Ag dressings on skin inflammation. J. Dermatol. 40 (6), 463–470.
Bjarnsholt, T., Kirketerp-Møller, K., Jensen, P., Madsen, K.G., Phipps, R., Krogfelt, K., Høiby, N., Givskov, M., 2008. Why chronic wounds will not heal: a novel hypothesis. Wound Repair Regen. 16 (1), 2–10.
Bjarnsholt, T., Buhlin, K., Dufrêne, Y.F., Gomelsky, M., Moroni, A., Ramstedt, M., Rumbaugh, K.P., Schulte, T., Sun, L., Åkerlund, B., Römling, U., 2018. Biofilm formation - what we can learn from recent developments. J. Intern. Med. 284 (4), 332–345.
Brunt, E.M., Janney, C.G., Di Bisceglie, A.M., Neuschwander-Tetri, B.A., Bacon, B.R., 1999. Nonalcoholic steatohepatitis: a proposal for grading and staging the histological lesions. Offi. J. Am. College Gastroenterol.| ACG 94 (9), 2467–2474.
Carter, D.A., Blair, S.E., Cokcetin, N.N., Bouzo, D., Brooks, P., Schothauer, R., Harry, E.J., 2016. Therapeutic manuka honey: no longer so alternative. Front. Microbiol. 7, 569.
Celleno, L., 2018. Topical urea in skincare: A review. Dermatol. Ther. 31 (6), e12690.
Chen, W., Xue, Z., Wang, J., Jiang, J., Zhao, X., Mu, T., 2018. Investigation on the thermal stability of deep eutectic solvents. Acta Phys. Chim. Sin 34 (8), 904–911.
Chen, Y., Yu, Q., Xu, C.-B., 2017. A convenient method for quantifying collagen fibers in atherosclerotic lesions by ImageJ software. Int. J. Clin. Exp. Med. 10 (10), 14904–14910.
El-Sayed, S.E., Abdelaziz, N.A., El-Housseiny, G.S., Aboshanab, K.M., 2024. Nanosponge hydrogel of octadecyl 3-(3,5-di-tert-butyl-4-hydroxyphenyl) propanoate of Alcaligenes faecalis. Appl. Microbiol. Biotechnol. 108 (1), 100.
Eriksson, E., Liu, P.Y., Schultz, G.S., Martins-Green, M.M., Tanaka, R., Weir, D., Gould, L. J., Armstrong, D.G., Gibbons, G.W., Wolcott, R., Olutoye, O.O., Kirsner, R.S., Gurtner, G.C., 2022. Chronic wounds: Treatment consensus. Wound Repair Regen. 30 (2), 156–171.
Ezquer, F., Giraud-Billoud, M., Carpio, D., Cabezas, F., Conget, P., Ezquer, M., 2015. Proregenerative microenvironment triggered by donor mesenchymal stem cells preserves renal function and structure in mice with severe diabetes mellitus. Biomed. Res. Int. 2015, 164703.
Ezquer, M., Urzua, C.A., Montecino, S., Leal, K., Conget, P., Ezquer, F., 2016. Intravitreal administration of multipotent mesenchymal stromal cells triggers a cytoprotective microenvironment in the retina of diabetic mice. Stem. Cell Res. Ther. 7, 42.
Flayhart, D., Lema, C., Borek, A., Carroll, K.C., 2004. Comparison of the BBL CHROMagar Staph aureus agar medium to conventional media for detection of Staphylococcus aureus in respiratory samples. J. Clin. Microbiol. 42 (8), 3566–3569.
Forgacs, G., Newman, S.A., Hinner, B., Maier, C.W., Sackmann, E., 2003. Assembly of collagen matrices as a phase transition revealed by structural and rheologic studies. Biophys. J. 84 (2), 1272–1280.
Franks, F., 1995. Protein destabilization at low temperatures. Adv. Protein Chem. 46, 105–139.
Ganguly, P., Bubák, D., Polák, J., Fagan, P., Dračínský, M., van der Vegt, N.F.A., Heyda, J., Shea, J.-E., 2022. Cosolvent exclusion drives protein stability in trimethylamine N-oxide and betaine solutions. J. Phys. Chem. Lett. 13 (34), 7980–7986.
Garcia-Bilbao, A., Gómez-Fernández, P., Larush, L., Soroka, Y., Suarez-Merino, B., Frusic-Zlotkin, M., Magdassi, S., Goñi-de-Cerio, F., 2020. Preparation, characterization, and biological evaluation of retinyl palmitate and Dead Sea water loaded nanoemulsions toward topical treatment of skin diseases. J. Bioact. Compat. Polym. 35 (1), 24–38.
Hengzhuang, W., Wu, H., Ciofu, O., Song, Z., Høiby, N., 2011. Pharmacokinetics/pharmacodynamics of colistin and imipenem on mucoid and nonmucoid Pseudomonas aeruginosa biofilms. Antimicrob Agents Chemother 55 (9), 4469–4474.
Jull, A.B., Cullum, N., Dumville, J.C., Westby, M.J., Deshpande, S., Walker, N., 2015. Honey as a topical treatment for wounds. Cochrane Database Syst. Rev. 2015 (3), Cd005083.
Kataoka, Y., Kunimitsu, M., Nakagami, G., Koudounas, S., Weller, C.D., Sanada, H., 2021. Effectiveness of ultrasonic debridement on reduction of bacteria and biofilm in patients with chronic wounds: A scoping review. Int. Wound J. 18 (2), 176–186.
Kawahira, K., 1999. Immunohistochemical staining of proliferating cell nuclear antigen (PCNA) in malignant and nonmalignant skin diseases. Arch. Dermatol. Res. 291, 413–418.
Kou, Z., Li, B., Aierken, A., Tan, N., Li, C., Han, M., Jing, Y., Li, N., Zhang, S., Peng, S., Zhao, X., Hua, J., 2023. Mesenchymal stem cells pretreated with collagen promote skin wound-healing. Int. J. Mol. Sci. 24 (10).
Krishnan, N., Velramar, B., Ramatchandirin, B., Abraham, G.C., Duraisamy, N., Pandiyan, R., Velu, R.K., 2018. Effect of biogenic silver nanocubes on matrix metalloproteinases 2 and 9 expressions in hyperglycemic skin injury and its impact in early wound healing in streptozotocin-induced diabetic mice. Mater. Sci. Eng. C Mater. Biol. Appl. 91, 146–152.

Labronici, P.J., dos Santos-Viana, A.M., dos Santos-Filho, F.C., Santos-Pires, R.E., Labronici, G.J., Penteado-da Silva, L.h., 2016. Evaluación del dolor en el adulto mayor. Acta Ortop. Mex. 30 (2), 73–80.

Lewis, R., Whiting, P., ter Riet, G., O'Meara, S. and Glanville, J., 2001. A rapid and systematic review of the clinical effectiveness and cost-effectiveness of debriding agents in treating surgical wounds healing by secondary intention.

Liu, Y., Friesen, J.B., McAlpine, J.B., Lankin, D.C., Chen, S.N., Pauli, G.F., 2018. Natural deep eutectic solvents: properties, applications, and perspectives. J. Nat. Prod. 81 (3), 679–690.

Liu, Y.W., Wu, Y.J., Liu, J.M., Wang, W.X., Yang, Q.L., Yang, G.S., 2022. Deep eutectic solvents: Recent advances in fabrication approaches and pharmaceutical applications. Int. J. Pharm. 622.

Marhoffer, W., Stein, M., Maeser, E., Federlin, K., 1992. Impairment of polymorphonuclear leukocyte function and metabolic control of diabetes. Diabetes Care 15 (2), 256–260.

Martins, M.A.R., Pinho, S.P., Coutinho, J.A.P., 2019. Insights into the nature of eutectic and deep eutectic mixtures. J. Solution Chem. 48 (7), 962–982.

Mecham, R.P., Birk, D.E., 2013. Extracellular matrix assembly and structure. Academic press.

Milne, J., 2015. Wound-bed preparation: the importance of rapid and effective desloughing to promote healing. Br. J. Nurs. 24 (Suppl 20), S52–S58.

Milne, J., Searle, R., Styche, T., 2020. The characteristics and impact of hard-to-heal wounds: results of a standardised survey. J. Wound Care 29 (5), 282–288.

Moormeier, D.E., Bayles, K.W., 2017. Staphylococcus aureus biofilm: a complex developmental organism. Mol. Microbiol. 104 (3), 365–376.

Mouës, C.M., Vos, M.C., Van Den Bemd, G.J.C.M., Stijnen, T., Hovius, S.E.R., 2004. Bacterial load in relation to vacuum-assisted closure wound therapy: a prospective randomized trial. Wound Repair Regen. 12 (1), 11–17.

Olivares, B., Martínez, F., Rivas, L., Calderón, C., Munita, J.M., Campodonico, P.R., 2018. A natural deep eutectic solvent formulated to stabilize β-lactam antibiotics. Sci. Rep. 8 (1), 14900.

Olivares, B., Martínez, F.A., Ezquer, M., Morales, B.J., Fuentes, I., Calvo, M., Campodónico, P.R., 2022. Betaine-urea deep eutectic solvent improves imipenem antibiotic activity. J. Mol. Liq. 350, 118551.

Percival, S.L., Suleman, L., 2015. Slough and biofilm: removal of barriers to wound healing by desloughing. J Wound Care 24 (11), 498–510.

Price, B.L., Lovering, A.M., Bowling, F.L., Dobson, C.B., 2016. Development of a novel collagen wound model to simulate the activity and distribution of antimicrobials in soft tissue during diabetic foot infection. Antimicrob Agents Chemother 60 (11), 6880–6889.

Quan, K., Hou, J., Zhang, Z., Ren, Y., Peterson, B.W., Flemming, H.-C., Mayer, C., Busscher, H.J., van der Mei, H.C., 2022. Water in bacterial biofilms: pores and channels, storage and transport functions. Crit. Rev. Microbiol. 48 (3), 283–302.

Rajhathy, E.M., Chaplain, V., Hill, M.C., Woo, K.Y., Parslow, N.E., 2021. Executive Summary: debridement: Canadian best practice recommendations for nurses developed by Nurses Specialized in Wound, Ostomy and Continence Canada (NSWOCC). J. Wound Ostomy Cont. Nurs. 48 (6), 516–522.

Ran, Y., Su, W., Ma, L., Wang, X., Li, X., 2021. Insight into the effect of sulfonated chitosan on the structure, rheology and fibrillogenesis of collagen. Int. J. Biol. Macromol. 166, 1480–1490.

Rötzer, V., Hartlieb, E., Winkler, J., Walter, E., Schlipp, A., Sardy, M., Spindler, V., Waschke, J., 2016. Desmoglein 3-dependent signaling regulates keratinocyte migration and wound healing. J. Invest. Dermatol. 136 (1), 301–310.

Sánchez, P.B., González, B., Salgado, J., José Parajó, J., Domínguez, Á., 2019. Physical properties of seven deep eutectic solvents based on l-proline or betaine. J. Chem. Thermodyn. 131, 517–523.

Sauer, K., Cullen, M.C., Rickard, A.H., Zeef, L.A.H., Davies, D.G., Gilbert, P., 2004. Characterization of nutrient-induced dispersion in Pseudomonas aeruginosa PAO1 biofilm. J. Bacteriol. 186 (21), 7312–7326.

Section 2. Evolving the notion of Wound Hygiene, Journal of Wound Care 31(4) (2022) S8-S12.

Sen, C.K., Roy, S., Mathew-Steiner, S.S., Gordillo, G.M., 2021. Biofilm management in wound care. Plast. Reconstr. Surg. 148 (2), 275e–e288.

Shi, L., Ermis, R., Lam, K., Cowart, J., Attar, P., Aust, D., 2009. Study on the debridement efficacy of formulated enzymatic wound debriding agents by in vitro assessment using artificial wound eschar and by an in vivo pig model. Wound Repair Regen. 17 (6), 853–862.

Shishov, A., Melesova, M., Bulatov, A., 2023. Three-component deep eutectic solvent-based microextraction approach for biodiesel quality control: Determination of water and metals. Anal. Chim. Acta 1277, 341658.

Stasiulewicz, M., Panuszko, A., Śmiechowski, M., Bruździak, P., Maszota, P., Stangret, J., 2021. Effect of urea and glycine betaine on the hydration sphere of model molecules for the surface features of proteins. J. Mol. Liq. 324, 115090.

Stewart, P.S., Costerton, J.W., 2001. Antibiotic resistance of bacteria in biofilms. Lancet 358 (9276), 135–138.

Stuart, K., Panitch, A., 2008. Influence of chondroitin sulfate on collagen gel structure and mechanical properties at physiologically relevant levels. Biopolymers 89 (10), 841–851.

Sun, X.Y., Yu, J.M., Wei, Q.F., Ren, X.L., 2023. Construction of chitosan-based supramolecular biofilm material for wound dressing based on natural deep eutectic solvents. Int. J. Biol. Macromol. 236.

Swanson, T., Ousey, K., Haesler, E., Bjarnsholt, T., Carville, K., Idensohn, P., Kalan, L., Keast, D.H., Larsen, D., Percival, S., Schultz, G., Sussman, G., Waters, N., Weir, D., 2022. IWII Wound Infection in Clinical Practice consensus document: 2022 update. J. Wound Care 31 (Sup12), S10–S21.

The rationale for wound hygiene, Journal of Wound Care 29(3) (2020) S5-S10.

Thomas, D.C., Tsu, C.L., Nain, R.A., Arsat, N., Fun, S.S., Lah, N., 2021. The role of debridement in wound bed preparation in chronic wound: A narrative review. Annal. Med. Surgery 71, 7.

Wang, C., Guo, M., Zhang, N., Wang, G., 2019. Effectiveness of honey dressing in the treatment of diabetic foot ulcers: A systematic review and meta-analysis. Complement Ther. Clin. Pract. 34, 123–131.

Wang, K., Hao, Y., Wang, Y., Chen, J., Mao, L., Deng, Y., Chen, J., Yuan, S., Zhang, T., Ren, J., 2019. Functional hydrogels and their application in drug delivery, biosensors, and tissue engineering. Int. J. Poly. Sci. 2019, 1–14.

Wijayapala, R., Hashemnejad, S.M., Kundu, S., 2017. Carbon nanodots crosslinked photoluminescent alginate hydrogels. RSC Adv. 7 (79), 50389–50395.

Wilkinson, H.N., McBain, A.J., Stephenson, C., Hardman, M.J., 2016. Comparing the effectiveness of polymer debriding devices using a porcine wound biofilm model. Adv. Wound Care 5 (11), 475–485.

Woo, K.Y., Keast, D., Parsons, N., Sibbald, R.G., Mittmann, N., 2015. The cost of wound debridement: a Canadian perspective. Int. Wound J. 12 (4), 402–407.

Woodard, L.N., Grunlan, M.A., 2018. Hydrolytic degradation and erosion of polyester biomaterials. ACS Publ.

Wu, X., Xu, R., Ren, Q., Bai, J., Zhao, J., 2012. Factors affecting extracellular and intracellular polysaccharide production in submerged cultivation of Tricholoma mongolicum. Afr. J. Microbiol. Res. 6 (5), 909–916.

Yilmaz, A.C., Aygin, D., 2020. Honey dressing in wound treatment: a systematic review. Complement. Ther. Med. 51, 102388.

Zheng, Q., Zhang, Y., Montazerian, M., Gulbiten, O., Mauro, J.C., Zanotto, E.D., Yue, Y., 2019. Understanding glass through differential scanning calorimetry. Chem. Rev. 119 (13), 7848–7939.

Zhu, N., Qian, F., Xu, X., Wang, M., Teng, Q., 2021. Thermogravimetric experiment of urea at constant temperatures. Materials 14 (20), 6190.

Zou, Z., Zhang, Z., Ren, H., Cheng, X., Chen, X., He, C., 2023. Injectable antibacterial tissue-adhesive hydrogel based on biocompatible o-phthalaldehyde/amine crosslinking for efficient treatment of infected wounds. Biomaterials 301, 122251.